14-YEAR PROGRAM MONITORING THE FLUX DENSITIES OF 33 RADIO SOURCES AT LOW FREQUENCIES

José Francisco Salgado,[1] Daniel R. Altschuler,[2] Tapasi Ghosh,[2] Brian K. Dennison,[3]
Kenneth J. Mitchell,[4] and Harry E. Payne[5]

ABSTRACT

We present the results of a low-frequency flux density monitoring program of 33 extragalactic radio sources. The light curves at 318 and 430 MHz over a 14 yr period are presented. The measurements were made with the NAIC Arecibo 305 m radio telescope at approximately bimonthly intervals between 1980 January and 1989 February and at less regular intervals between 1989 October and 1993 October, for a total of 64 observing sessions. In addition, we provide a first discussion of the results, pointing out several source properties and interesting objects.

Subject headings: ISM: general — quasars: general — radio continuum: galaxies

1. INTRODUCTION

The radio intensity variability of active galactic nuclei (AGNs) has been the subject of extensive study since its discovery by Dent (1965) and Sholomitskii (1965). The short timescales of variability of a few months at centimetric wavelengths implied such high brightness temperatures in these compact sources that bulk relativistic motions of the synchrotron-emitting plasma at angles close to the line of sight had to be invoked (for a review see Altschuler 1989). To date, the most successful models for explaining such phenomena involve relativistic shocks propagating in radio jets (Königl & Choudhuri 1985; Hughes, Aller, & Aller 1989; Marscher 1992). The subsequent discoveries of low-frequency variability (<1 GHz) and intraday variability have pushed these models to their extremes. The current scenarios suggest that low-frequency variability is mostly caused by refractive interstellar scintillation (RISS, for a review, see Rickett 1986 and references therein), while for sources showing intraday variability, the observer appears to be probing the very inner jet, where the fluid is likely to be highly relativistic (Wagner et al. 1996).

Between 1980 and 1993, we monitored 33 compact extragalactic radio sources at 318 and 430 MHz using the NAIC Arecibo 305 m radio telescope. Results for 1980 January to 1984 December have been reported in Mitchell et al. (1994, hereafter Paper I), and discussions of selected sources can be found in Altschuler et al. (1984), Dennison et al. (1984), and O'Dell et al. (1988). Here we present the data observed subsequent to 1984. In § 2 we describe the observational procedure and data reduction for the sessions between 1984 and 1993. In §§ 3–5 we present "light curves" with all the measurements since 1980 January and provide a first discussion of the results, pointing out several source properties and interesting objects. The theory of RISS predicts a dependence between source structure and variability

properties, which led to the VLBI measurements of a subsample of our sources. These results are the subject of a separate study (Altschuler et al. 1995).

2. SAMPLE AND OBSERVATIONS

We selected 33 compact extragalactic sources that were known to be, or suspected of being, variable at low frequencies (Condon et al. 1979; Dennison et al. 1981). These are listed in Table 1. In this table, columns (3)–(6) give the source positions in equatorial and Galactic coordinates. The redshifts, where known, are listed in column (7). Optical identifications are presented in column (8), where G stands for galaxy, Q for quasar, B for BL Lac object, HPQ for quasars with high (>3%) optical polarization, and Sey 2 for type 2 Seyfert galaxy.

In addition to these sources, eight standard Arecibo flux density calibrators were observed in identical fashion to the sample sources. These are listed in the lower section of Table 1.

We used the Arecibo 305 m radio telescope in drift-scan mode at approximately bimonthly intervals between 1980 and 1989 and at less regular intervals between 1989 and 1993, for a total of 64 observing sessions. Internal calibration was achieved by switching on a signal of constant strength for a short interval at the beginning of each drift scan. Each source was always observed at the same sidereal time (hour angle) in order to reproduce the confusion contribution to the scan and to minimize the residual errors due to the zenith angle-gain calibration. A single polarization was recorded at each frequency, linear at 318 MHz and circular at 430 MHz.

To estimate the flux densities, we fitted Gaussians to the drift scans of the source. Scans were inspected visually and corrections to the baseline were made as required. Care was taken to ensure consistency in the measurements of a given source at a given frequency over the 14 yr. Scans with serious problems, such as those containing strong terrestrial/solar interference or ionospheric/interplanetary scintillations, were rejected.

The heights of the fitted Gaussians were normalized by the internal noise calibration and corrected for antenna gain. For the 305 m antenna, the gain depends upon the zenith angle (ZA) of the observation, and to a much smaller extent on the feed platform elevation, which varies because of thermal expansion of the support cables. Finally, the

[1] Department of Astronomy, University of Michigan, Ann Arbor, MI 481091-1090; salgado@astro.lsa.umich.edu.
[2] National Astronomy and Ionosphere Center-Arecibo Observatory, H3 Box 53995, Arecibo, PR 00612; daniel@naic.edu, tghosh@naic.edu.
[3] Department of Physics, Virginia Polytechnic Institute and State University, Blacksburg, VA 24061; dennison@astro.phys.vt.edu.
[4] General Sciences Corporation, 4600 Power Mill Rd, Suite 400, Bettsville, MD, 20705-2675; mitchell@stars.dnet.nasa.gov.
[5] Space Telescope Science Institute, 3700 San Martin Drive, Baltimore, MD 21218; payne@stsci.edu.

TABLE 1

MONITORED SOURCES

ID (1)	SOURCE (2)	α (1950.0)[a] (3)	δ (1950.0)[a] (4)	GALACTIC COORDINATES		z[a] (7)	TYPE[a] (8)
				l (deg) (5)	b (deg) (6)		
1.......	0038+328	00 38 13.8	32 53 41	120.1	−29.7	...	...
2.......	0056−001	00 56 31.8	−00 09 18	127.1	−62.4	...	...
3.......	0116+319	01 16 47.3	31 55 06	129.8	−30.3	...	G
4.......	0202+149	02 02 07.4	14 59 51	147.9	−44.0	...	...
5.......	0235+164	02 35 52.6	16 24 05	156.8	−39.1	0.94	B
6.......	0256+075	02 56 47.0	07 35 45	169.1	−43.3	0.89	Q
7.......	0316+162	03 16 09.1	16 17 41	166.6	−33.6	...	...
8.......	0333+321	03 33 22.3	32 08 37	159.0	−18.8	1.26	Q
9.......	0420−014	04 20 43.3	−01 27 28	194.0	−32.7	0.92	HPQ
10......	0446+112	04 46 21.2	11 16 19	187.4	−20.7	...	...
11......	0723−008	07 23 17.9	−00 48 55	216.2	8.0	0.13	B
12......	0735+178	07 35 14.1	17 49 09	201.9	18.1	>0.42	B
13......	0736+017	07 36 42.5	01 44 00	217.0	11.4	0.19	HPQ
14......	0851+202	08 51 57.3	20 17 58	206.8	35.8	0.31	B
15......	1039+029	10 39 04.2	02 58 15	245.5	50.5	...	...
16......	1055+018	10 55 55.4	01 50 03	251.5	52.8	0.89	HPQ
17......	1117+146	11 17 51.0	14 37 22	239.5	65.3	...	...
18......	1345+125	13 45 06.2	12 32 20	258.8	70.2	0.12	Sey 2
19......	1422+202	14 22 37.5	20 13 53	226.5	67.5	0.87	Q
20......	1548+056	15 48 07.0	05 36 11	231.8	42.2	1.42	Q
21......	1606+106	16 06 23.3	10 37 23	223.0	40.8	1.23	Q
22......	1611+343	16 11 48.0	34 20 19	55.2	46.4	1.40	Q
23......	1633+382	16 33 30.6	38 14 10	61.1	42.3	1.81	Q
24......	1901+319	19 01 02.4	31 55 14	63.0	11.8	0.64	Q
25......	1922+333	19 22 25.1	32 23 35	65.5	7.9	...	...
26......	2050+364	20 50 54.5	36 24 12	78.9	−5.1	...	G
27......	2144+092	21 44 42.5	09 15 51	65.8	−32.3	1.11	Q
28......	2145+067	21 45 36.1	06 43 40	63.7	−34.1	1.00	Q
29......	2201+315	22 01 01.4	31 31 08	86.0	−18.8	0.30	Q
30......	2223+210	22 23 14.8	21 02 51	83.2	−30.1	1.95	Q
31......	2230+114	22 30 07.8	11 28 23	77.4	−38.6	1.04	Q
32......	2251+158	22 51 29.5	15 52 54	86.1	−8.2	0.86	HPQ
33......	2319+272	23 19 31.8	27 16 18	99.7	−31.3	1.25	Q
Calibration Sources							
34......	0127+233	01 27 15.1	23 22 53	134.2	−38.4	1.47	Q
35......	0528+064	05 28 48.0	06 28 16	197.6	−14.5	...	...
36......	0710+118	07 10 15.6	11 51 20	204.8	10.1	0.77	Q
37......	1005+077	10 05 22.0	07 44 59	232.1	46.6	...	...
38......	1328+254	13 28 15.9	25 24 38	223.5	81.0	1.06	Q
39......	1328+307	13 28 49.7	30 45 59	56.5	80.7	0.85	Q
40......	1756+134	17 56 13.4	13 28 44	39.3	17.7	...	...
41......	2203+292	22 03 49.2	29 14 46	84.9	−20.9	4.41	Q

NOTE.—Units of right ascension are hours, minutes, and seconds, and units of declination are degrees, arcminutes, and arcseconds.

[a] Coordinates, redshifts and types from Véron-Cetty & Véron (1993), except the optical identification of 2050+364, from Biretta, Schneider, & Gunn (1985).

calibration sources were used to convert the gain-corrected responses into janskys. The flux density scale is based upon that of Baars et al. (1977). Details of the data reduction and error estimation procedures are described in Paper I and are not repeated here.

In practice, a slightly different data reduction procedure was used after the observing session of 1984 December. Following this session, the main modification was that a more rigorous calibration step height and baseline determination procedure was established. When we reanalyzed the 430 MHz data as a check, it led to a slight difference for some of the flux density values for the session of 1989

December of Paper I. Figure 1 shows a comparison where the values of Paper 1 and of the present paper are represented by S^a and S^b, respectively. The solid and dashed lines represent the mean and median values of S^b/S^a, 0.982 ± 0.009, and 0.998, respectively. The dotted lines represent the 3 σ confidence limits of the mean.

3. PRELIMINARY ANALYSIS

The light curves for the 33 sources monitored are displayed in Figure 2, where the individual flux densities have been normalized by the weighted mean over the entire monitoring period. Table 2 presents the results of our prelimi-
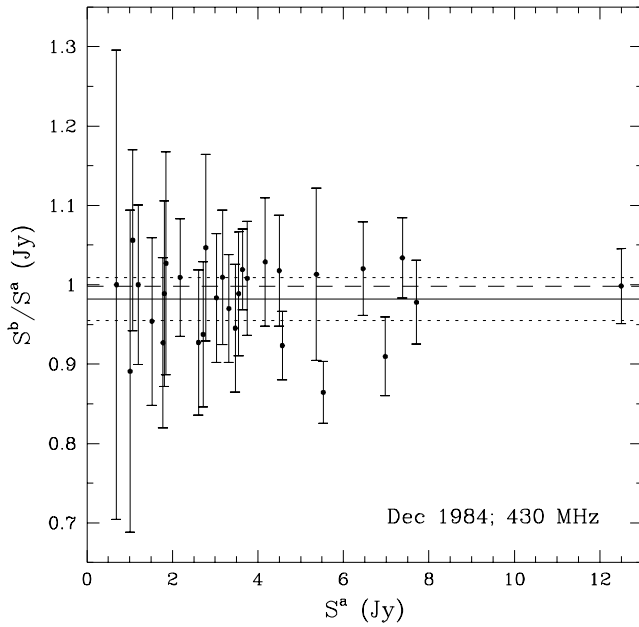
FIG. 1.—Comparison of flux density values determined by Mitchell et al. (1994), S^a, and Salgado et al. (this paper), S^b. The solid and dashed lines represent the mean and median values of S^b/S^a, 0.982 ± 0.009 and 0.998, respectively. The dotted lines represent the 3 σ confidence limits of the mean.

nary analysis of this data set. In columns (3) and (10) we list the mean flux densities ($\bar{S}$) at 318 and 430 MHz, respectively. For each source, we have also calculated modulation index (MI) and structure function (Σ) at both frequencies, as well as two-frequency cross-correlation functions.

3.1. Modulation Indices

For each source, modulation indices at both 318 and 430 MHz were calculated using MI = $\sigma_s/\bar{S}$, where σ_s is the rms flux density fluctuation over the entire monitoring period. These values are listed in columns (4) and (11) of Table 2.

In order to estimate the contribution of measurement errors to the values of modulation index for each source, we undertook the following error analysis. The total measurement error (σ_t) at any epoch is considered to be the quadratic sum of two independent factors:

$$\sigma_t^2 = \sigma_c^2 + \bar{S}^2 \sigma_g^2 , \tag{1}$$

where the flux density–independent term, σ_c, is mostly due to confusion and interference, while the flux density–dependent error, σ_g, is due to pointing errors as well as any error in gain estimation.

From straight-line fits to the plot of average values of σ_T^2 versus $\bar{S}^2$ of all sources, we estimated the values of σ_c and σ_g separately for the 318 and 430 MHz systems. For the line feed systems of the Arecibo Telescope, these errors fell into two sets—sources at low and at high zenith angles. The ZA values that divided the two sets were also frequency-dependent owing to the different designs of the two feeds. Table 3 summarizes the adopted values of σ_c and σ_g in the two ZA ranges at the two observing frequencies.

The modulation index due to measurement uncertainties alone was then computed for each source using

$$MI_c = \sigma_t/\bar{S} = \sqrt{\sigma_c^2/\bar{S}^2 + \sigma_g^2} . \tag{2}$$

In Figure 3 we present curves of the expected modulation indices due to noise as a function of flux density using equation (2), and the two σ-values in Table 3. Also drawn are curves of $2MI_c$ and $3MI_c$ versus flux density. The MI values actually measured (see Table 2) are superimposed. Sources falling above the $2MI_c$ curve were clearly variable during the monitoring period. However, we note that any long-term systematic change (often clearly correlated at both frequencies) may result in sources falling below the $2MI_c$ curve in Figure 3. In such cases, the above criterion fails to distinguish a variable source.

3.2. Structure-Function Analysis

Another technique for analyzing time series, which has been applied to low-frequency variablity studies by various authors (e.g., Spangler et al. 1993), is structure-function analysis. We computed the normalized structure function (Σ) for all sample sources using the relation

$$\Sigma(\tau) = \frac{1}{2\sigma^2} , \langle [S(t) - S(t + \tau)]^2 \rangle \tag{3}$$

where σ^2 is the variance of the flux density. We find that the normalized structure functions of these sources can be classified into four basic types, represented schematically in Figure 4. For sources with a type A structure function, a simple estimate of the timescale of variation has been made using the lag for which Σ rises to 0.77. Structure functions of types B and C are more complicated, and we believe that these are cases where two or more source components are varying independently. For nonvariable (NV) sources, the structure function rises to its saturation value of 1 within the first lag, while for slowly varying sources (type D) the structure function does not reach saturation even for the maximum computed lag of 7 yr. The structure functions of a few sources show a more complex nature that could not be classified according to the above-mentioned scheme. These are marked as U in Table 2.

Structure-function types for each source at both frequencies are entered in columns (5) and (2)1 of Table 2. For structure functions of type A, estimates of timescales are also listed in columns (6) and (13). Lower limits for the timescaled structure functions of type D are also given.

3.3. Correlated Variations at 318 and 430 MHz

We have also calculated cross-correlation functions between the 318 and 430 MHz data. If variations are intrinsic, an increasing time delay toward lower frequency could be expected, while for RISS no time delay is predicted. More detailed analysis involving source structures and propagation models will be presented in a future paper. Here we note only that most sources vary in a correlated fashion at these two frequencies. Exceptions are sources 5, 18, 19, and 31, which are variable at both frequencies but do not show any correlation. We note that source 22, 1611+343 is the most variable source in our sample, and the light curves at the two frequencies are highly correlated.

4. DISCUSSION

In Table 2, we indicated by crosses in the V_L, V_M, and V_Σ columns sources that can be identified as variable on the basis of a visual inspection of the light curves, modulation index studies, and structure-function analysis, respectively. In many cases, these three determinations are consistent.

1. 0038+328 [3C19]

2. 0056−001 [4C−00.06]

3. 0116+319 [4C31.04]
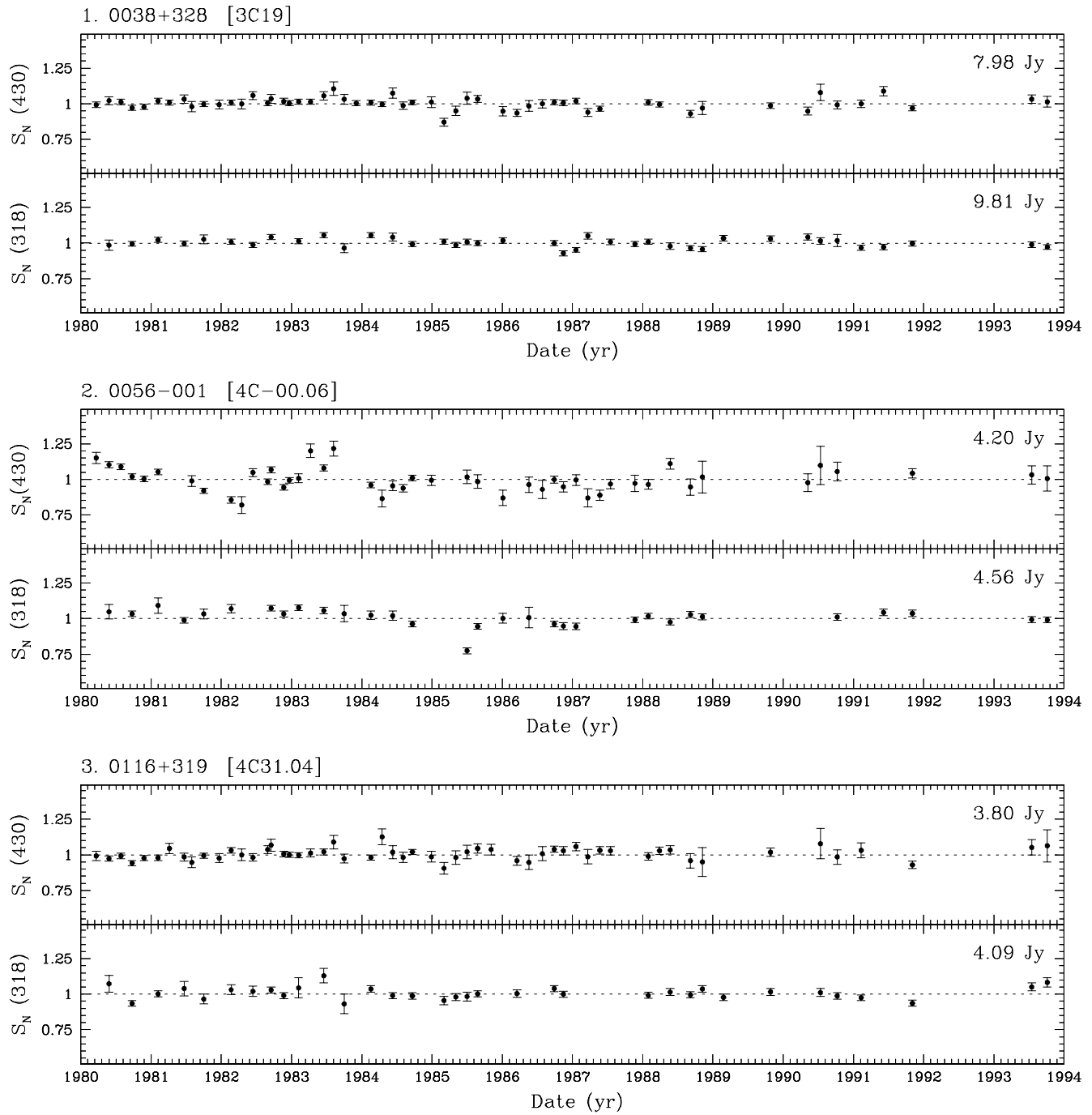
FIG. 2.—14-year radio "light curves" of the sources monitored at 318 and 430 MHz. *Abscissae*: date (yr); *ordinate*: flux density normalized by the weighted mean over the entire monitoring period; parameter: frequency (MHz). The weighted-mean flux density is given in the upper right-hand corner of each plot.
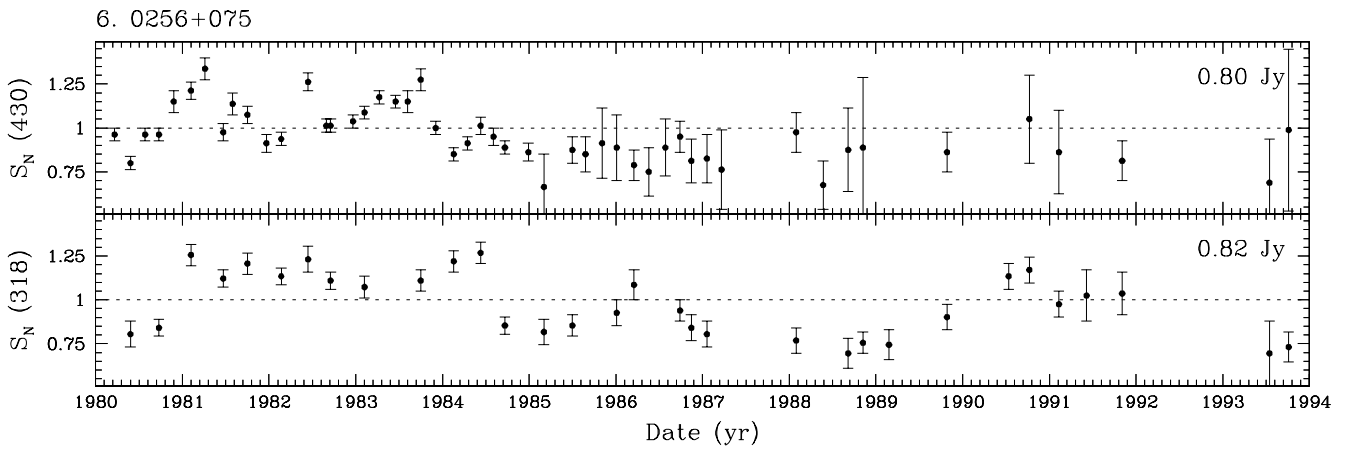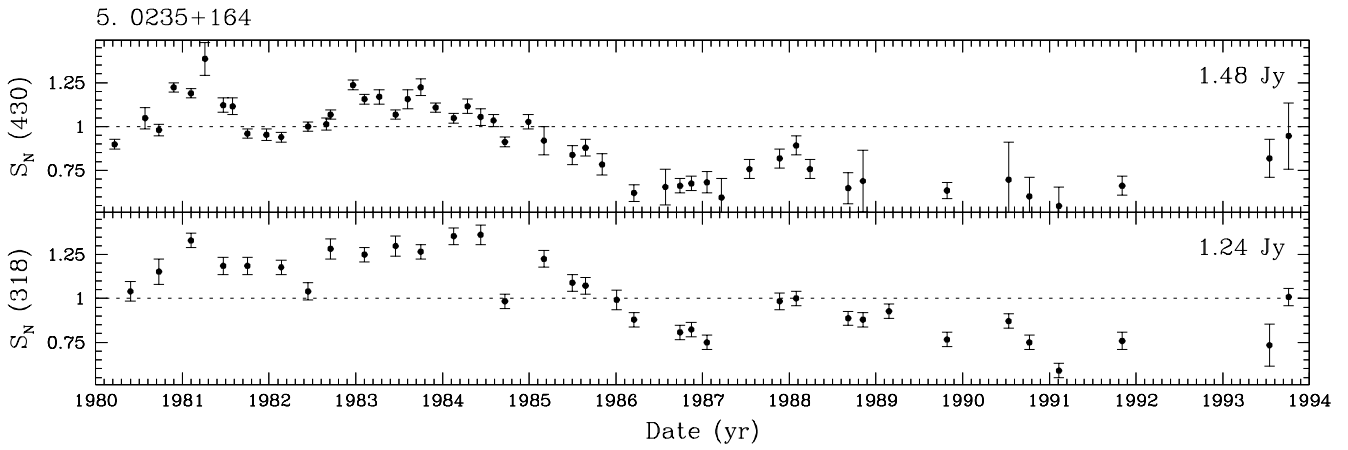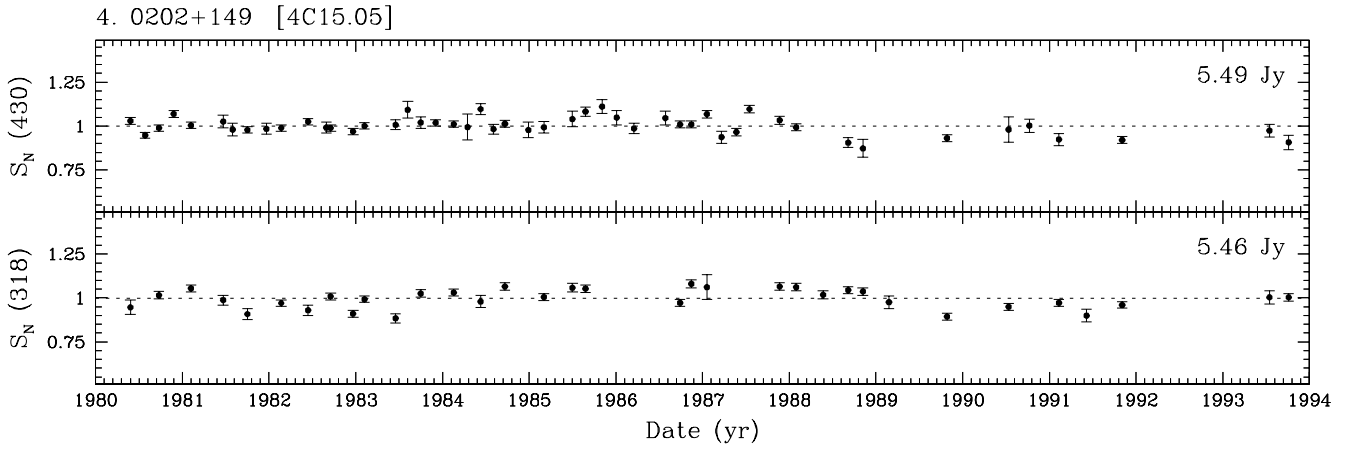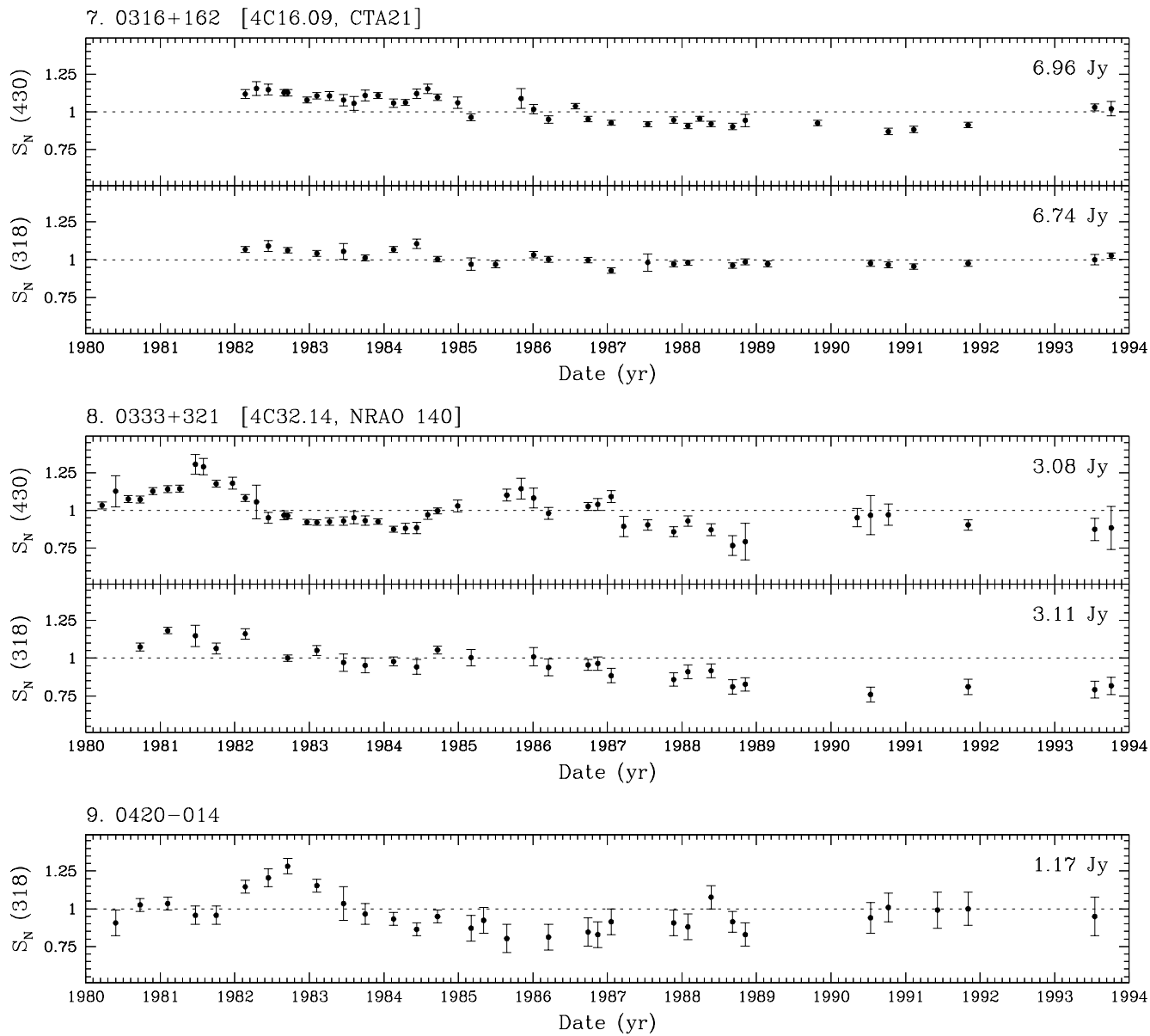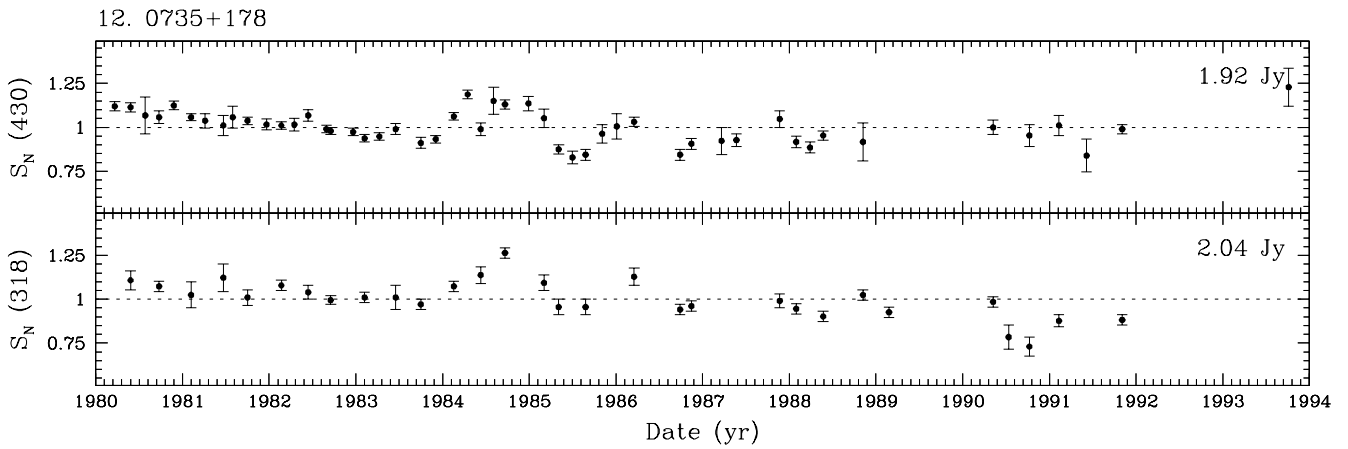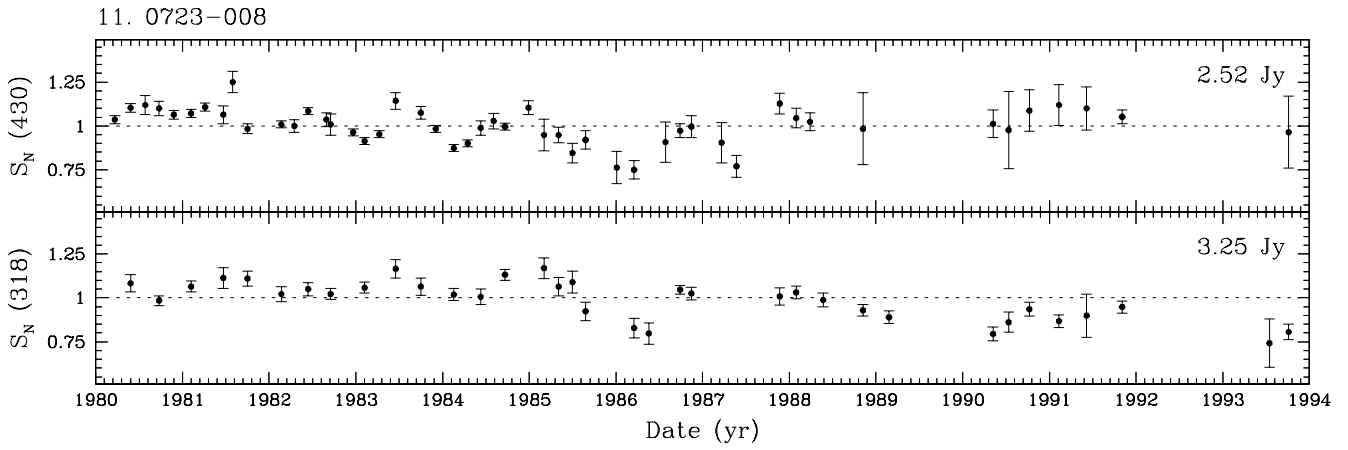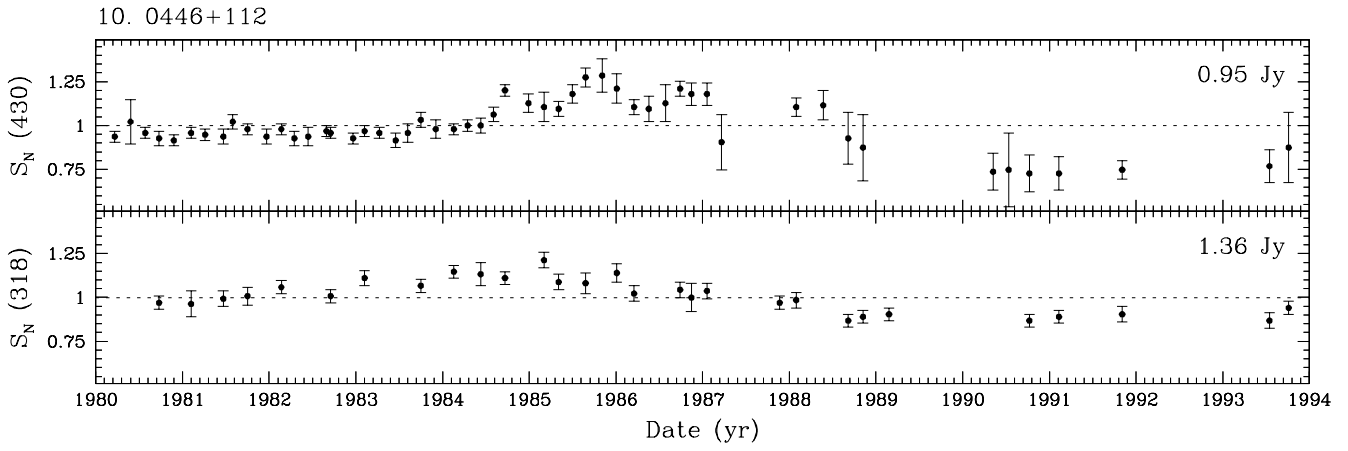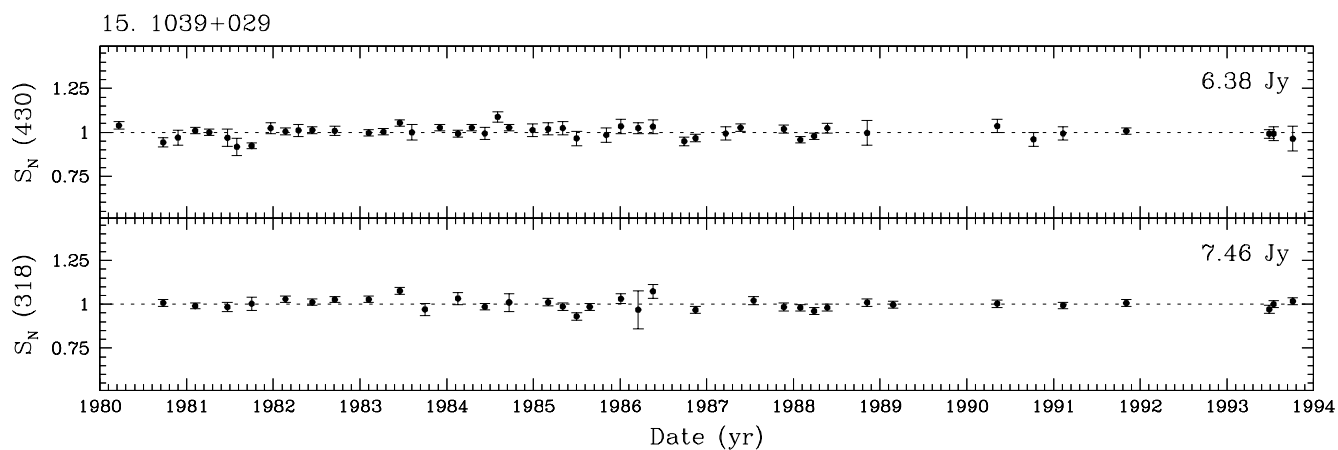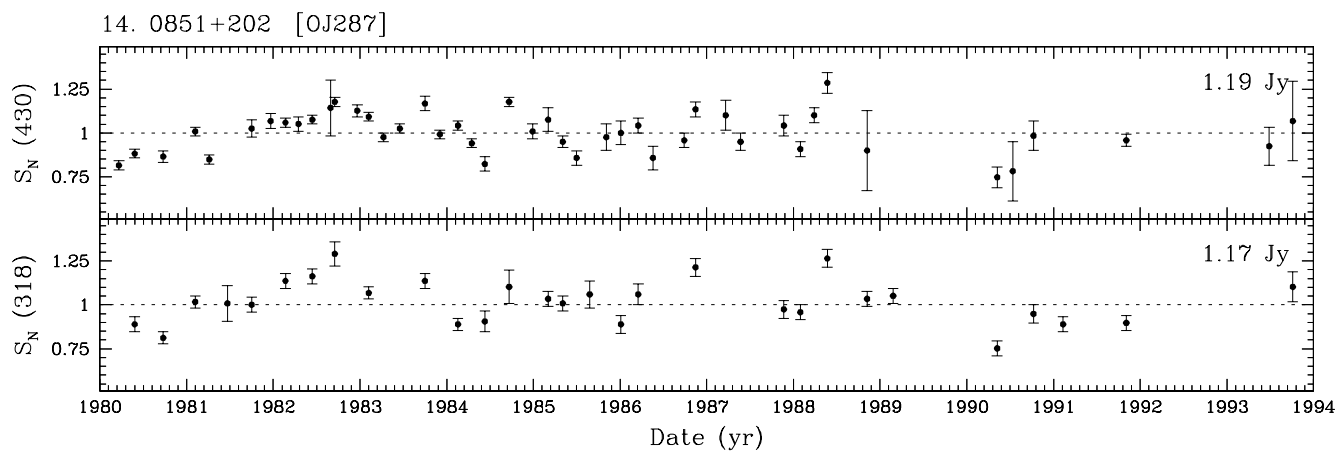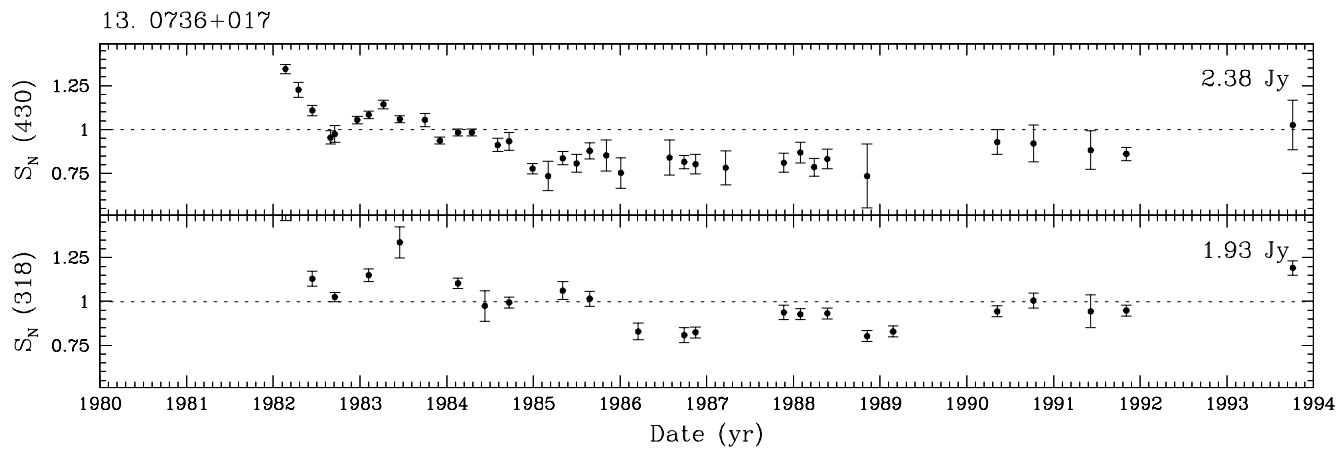
4. 0202+149 [4C15.05]

5. 0235+164

6. 0256+075

FIG. 2.—*Continued*

81

7. 0316+162 [4C16.09, CTA21]

8. 0333+321 [4C32.14, NRAO 140]

9. 0420−014

FIG. 2.—Continued

82

10. 0446+112

11. 0723−008

12. 0735+178

Fig. 2.—*Continued*

83

13. 0736+017

14. 0851+202 [OJ287]

15. 1039+029

Fig. 2.—*Continued*

16. 1055+018 [4C01.28]

17. 1117+146 [4C14.41]

18. 1345+125 [4C12.50]

Fig. 2.—*Continued*

85

19. 1422+202 [4C20.33]

20. 1548+056 [4C05.64]

21. 1606+106

Fig. 2.—*Continued*

86

22. 1611+343 [DA406]

2.90 Jy

3.37 Jy

23. 1633+382 [4C38.41]

0.69 Jy

2.16 Jy

24. 1901+319 [3C395]

5.11 Jy

6.08 Jy

FIG. 2.—*Continued*

25. 1922+333

26. 2050+364 [DA529]

27. 2144+092

Fig. 2.—*Continued*

88
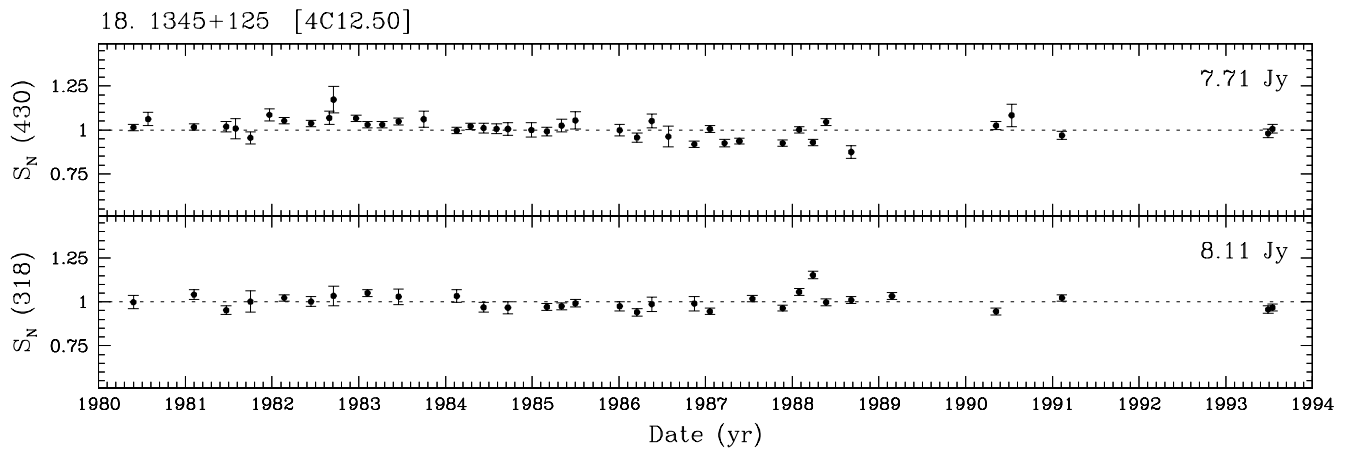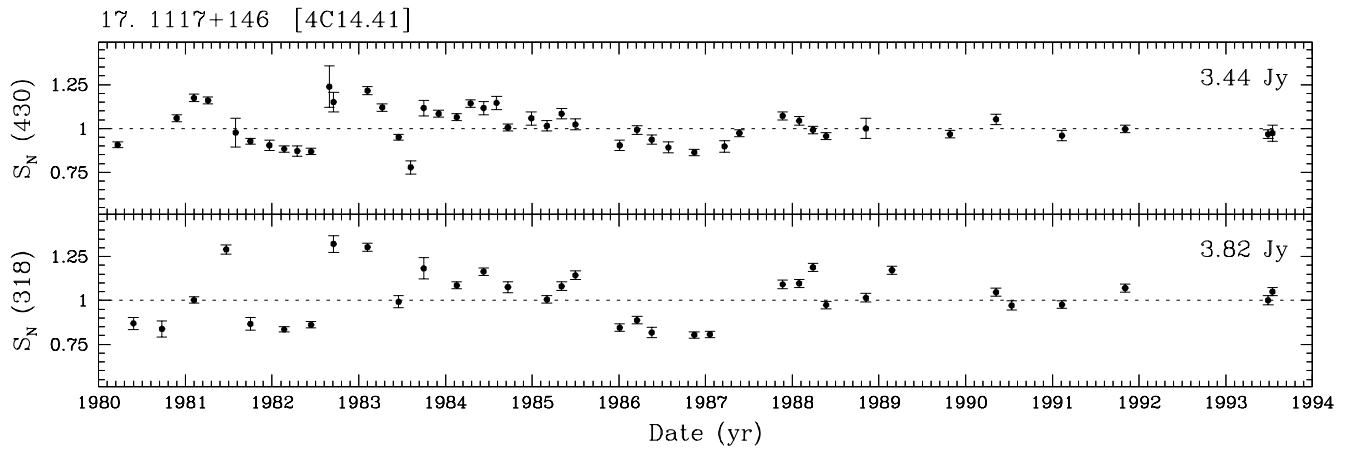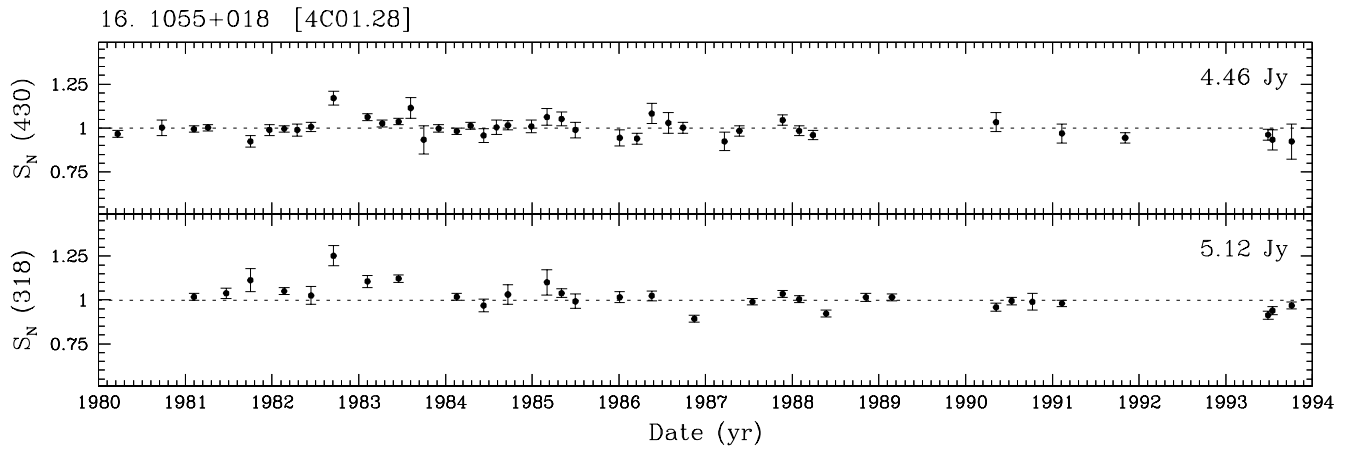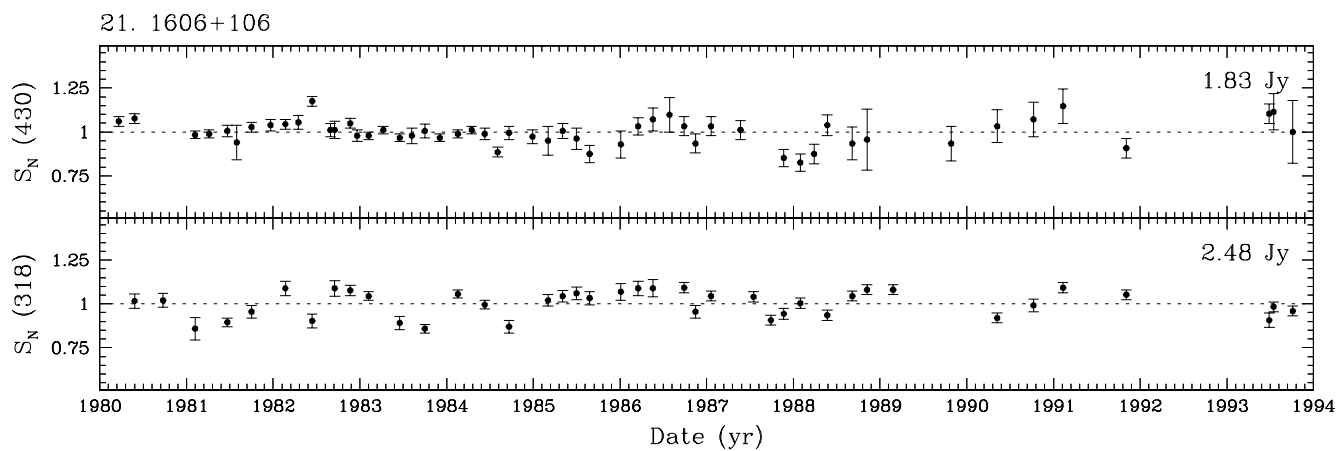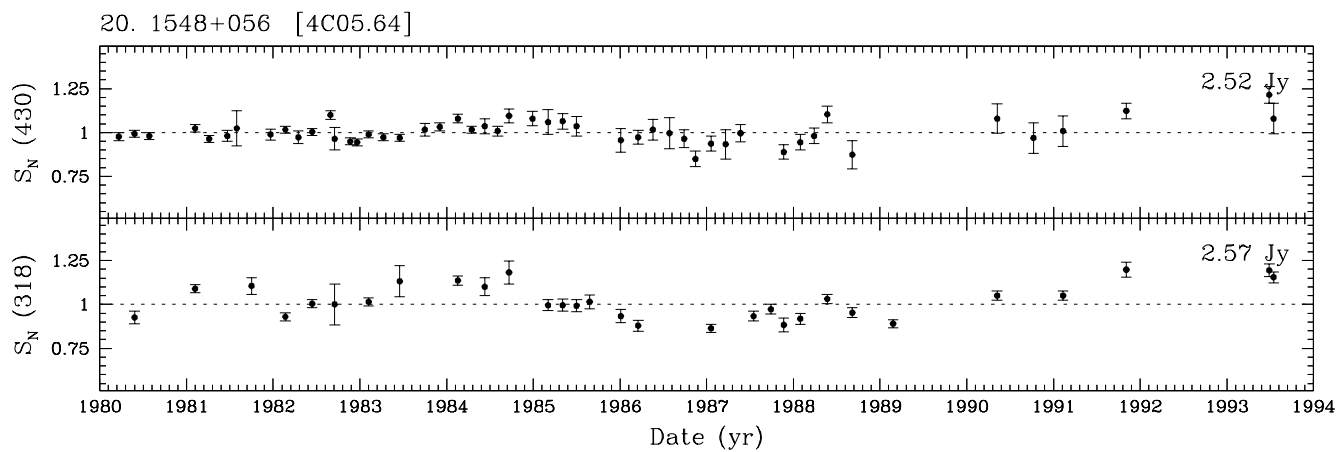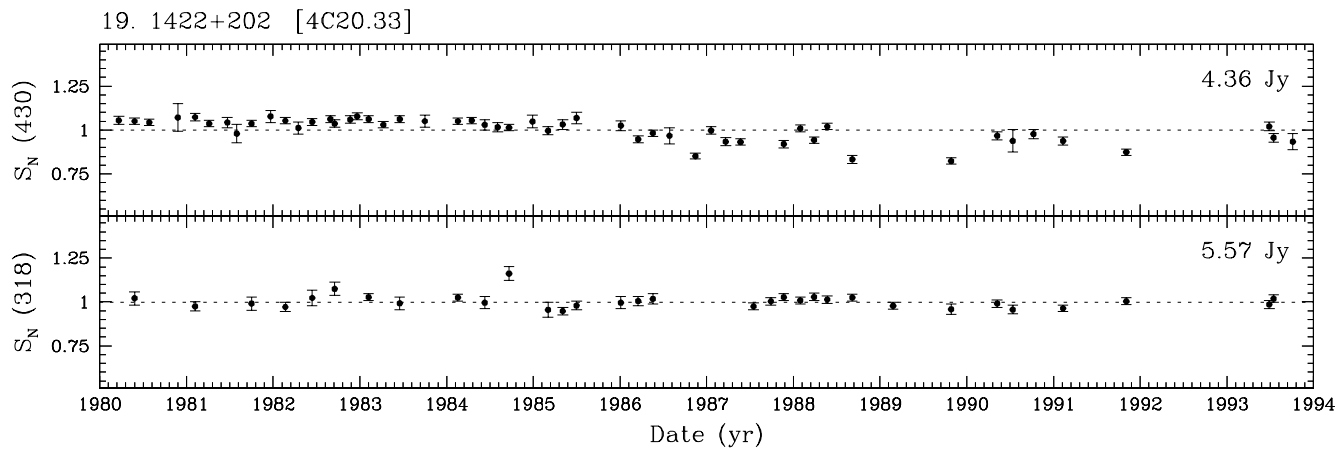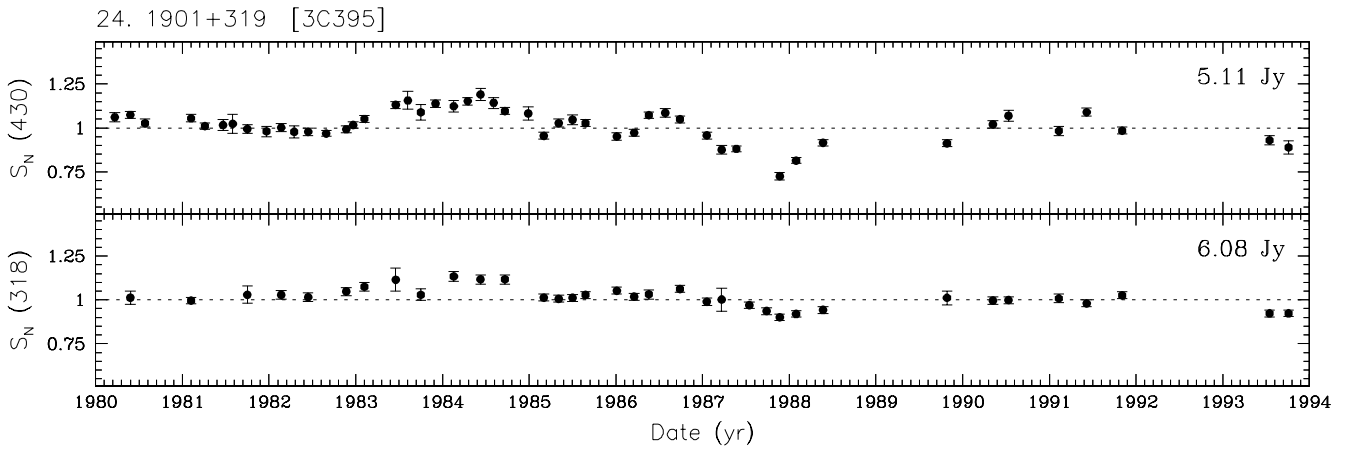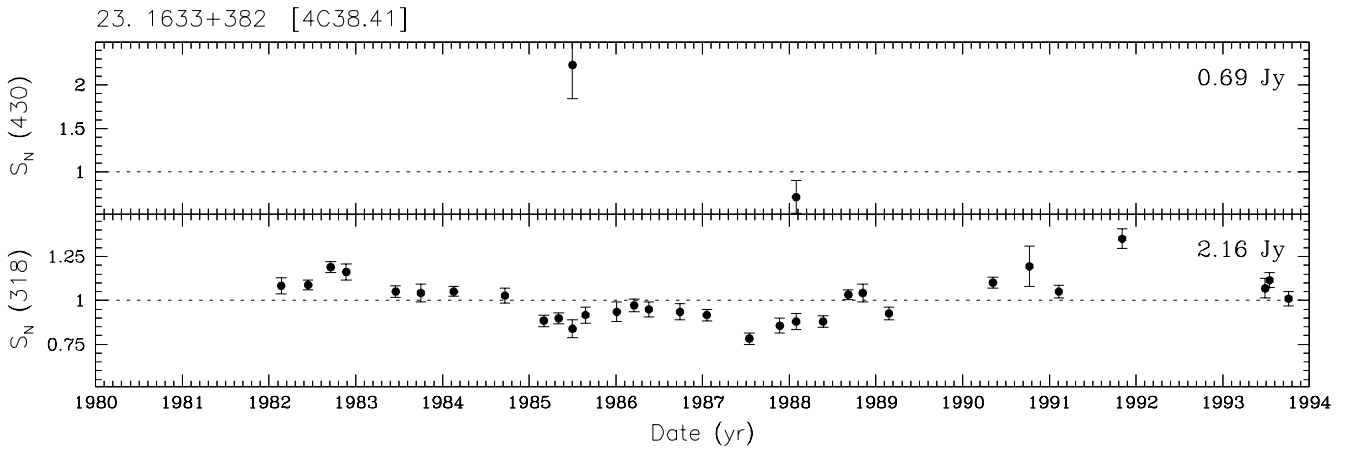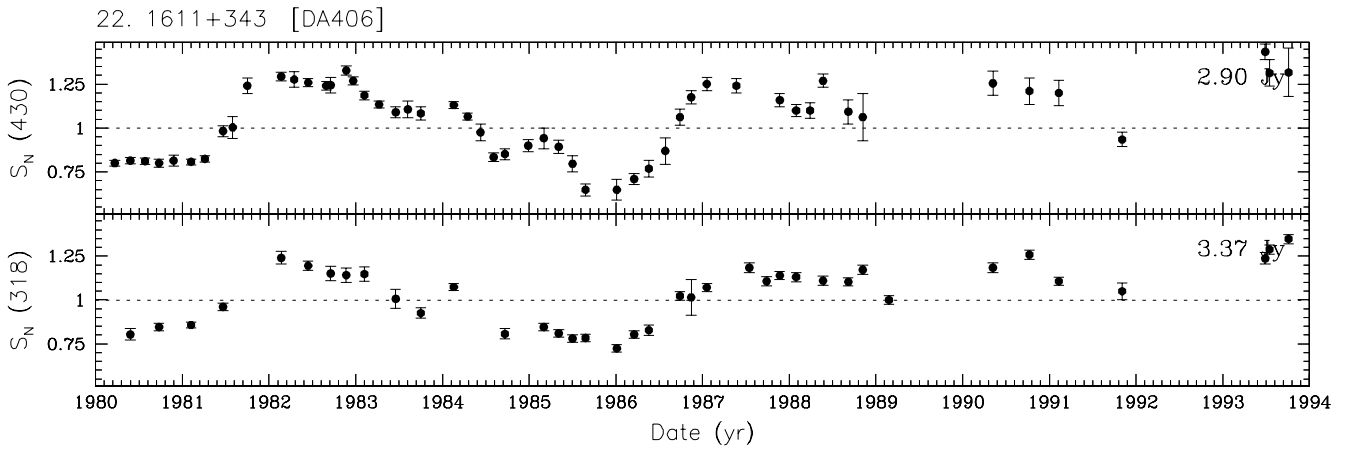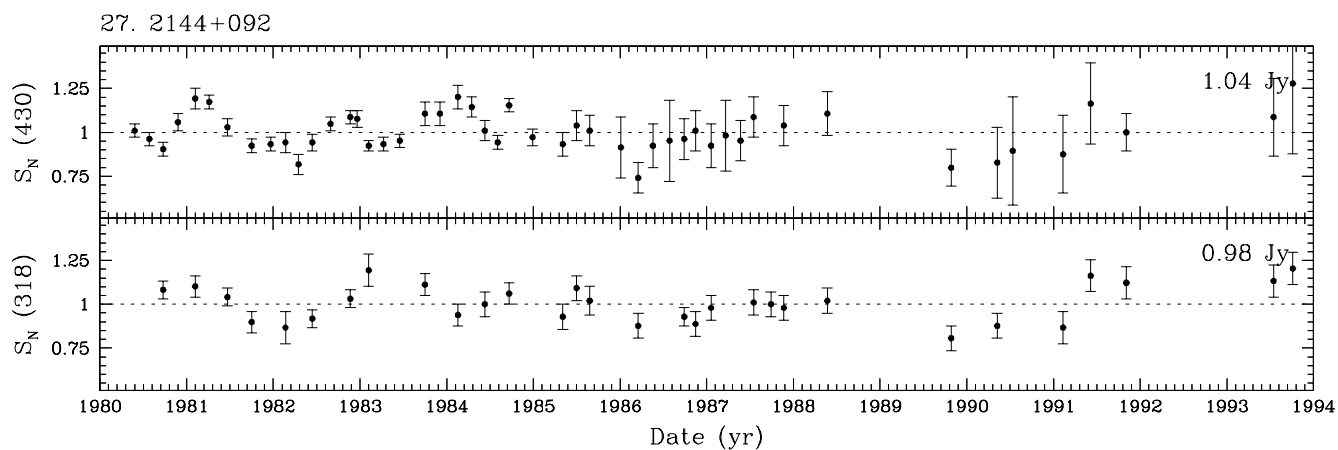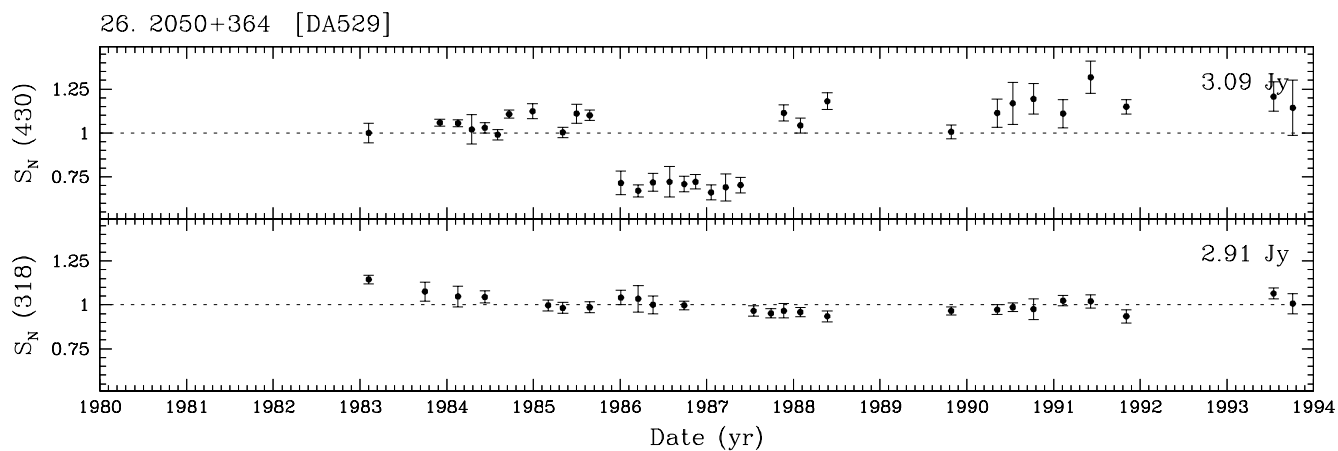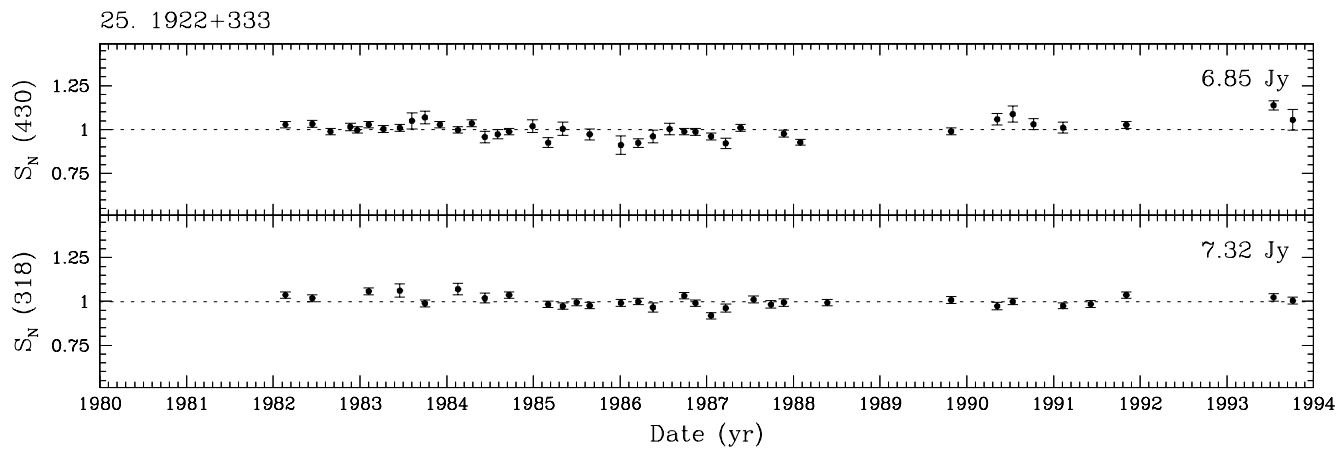
28. 2145+067 [4C06.69]
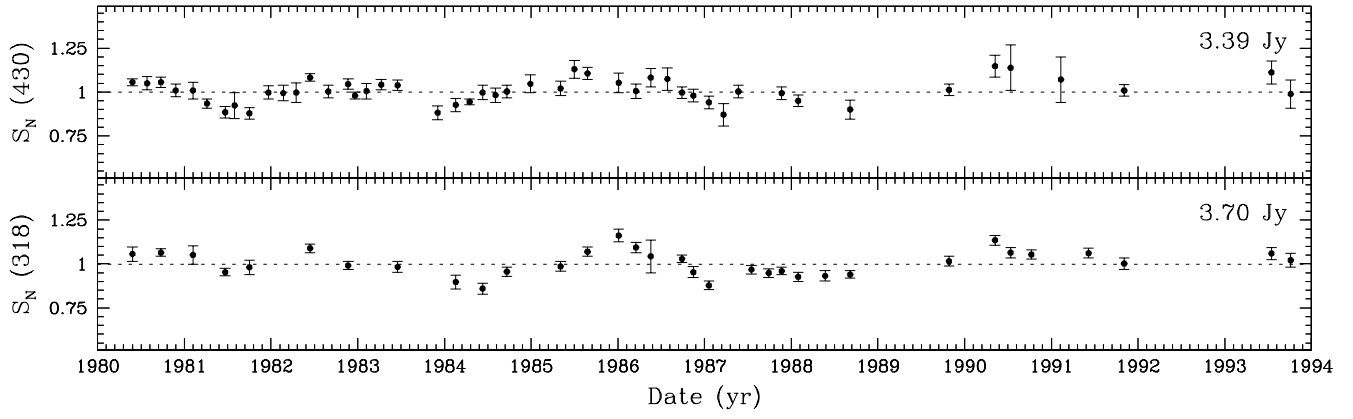
29. 2201+315 [4C31.63]
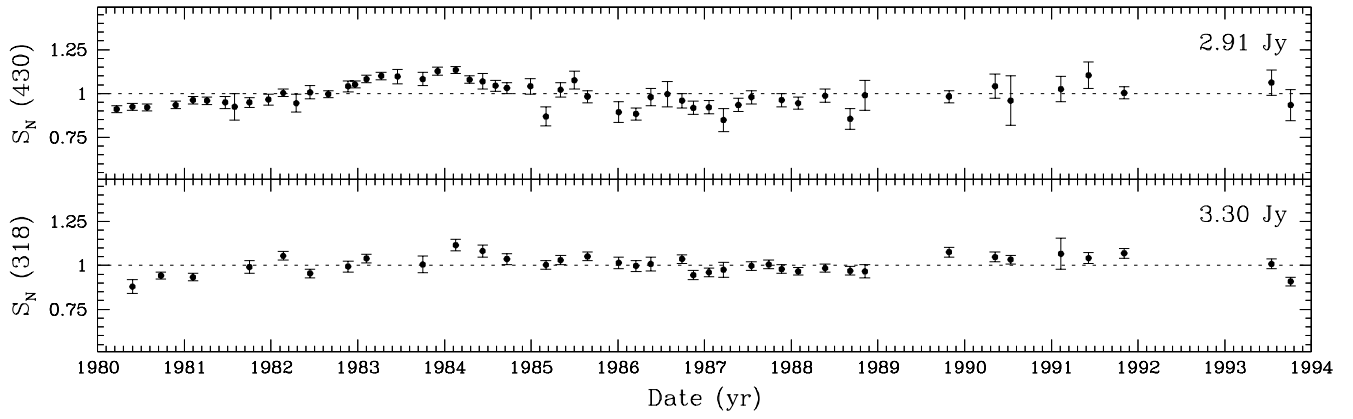
30. 2223+210

F_IG. 2.—*Continued*

31. 2230+114 [4C11.69]

FIG. 2.—*Continued*

32. 2251+158 [3C454.3]

33. 2319+272 [4C27.50]
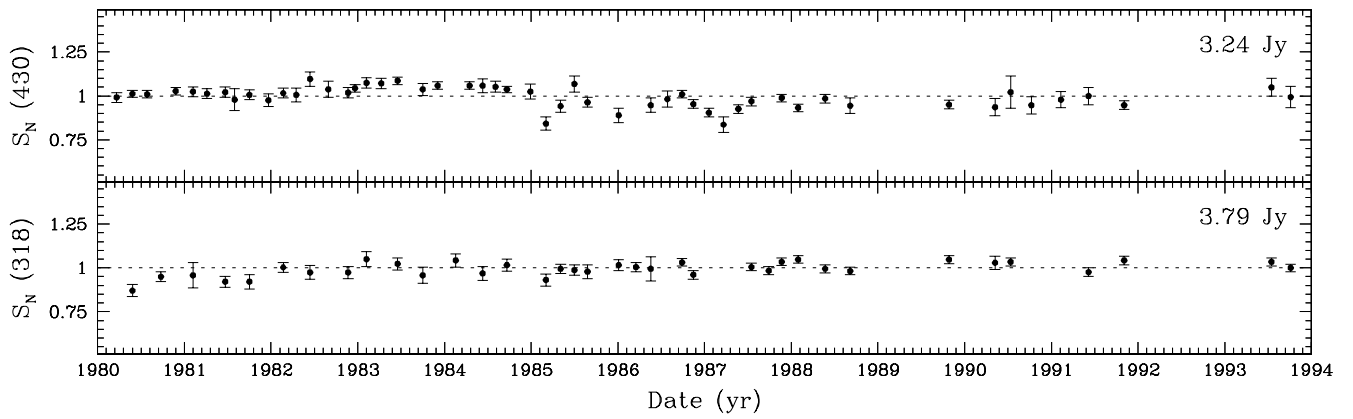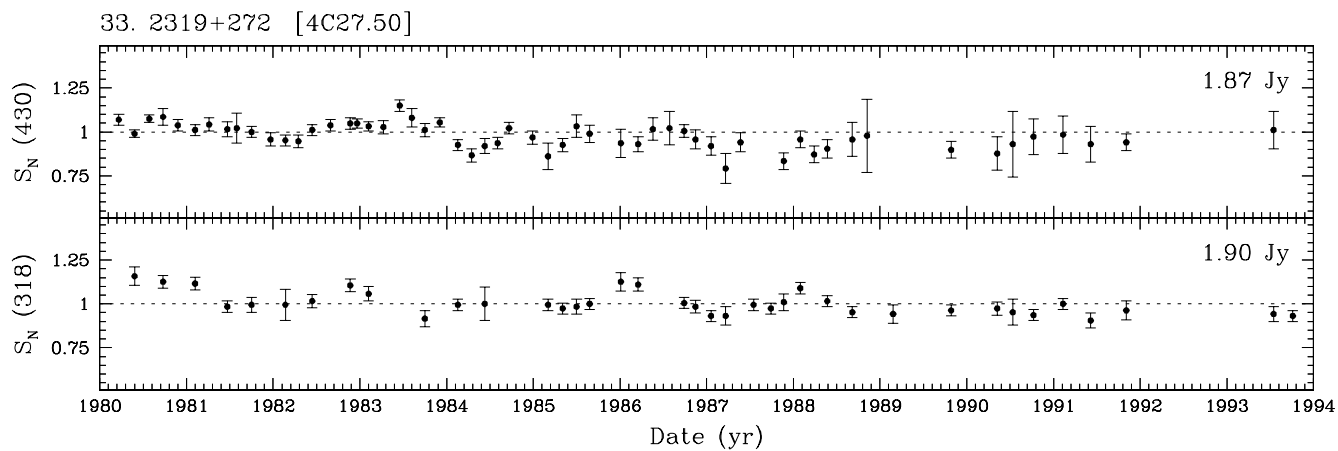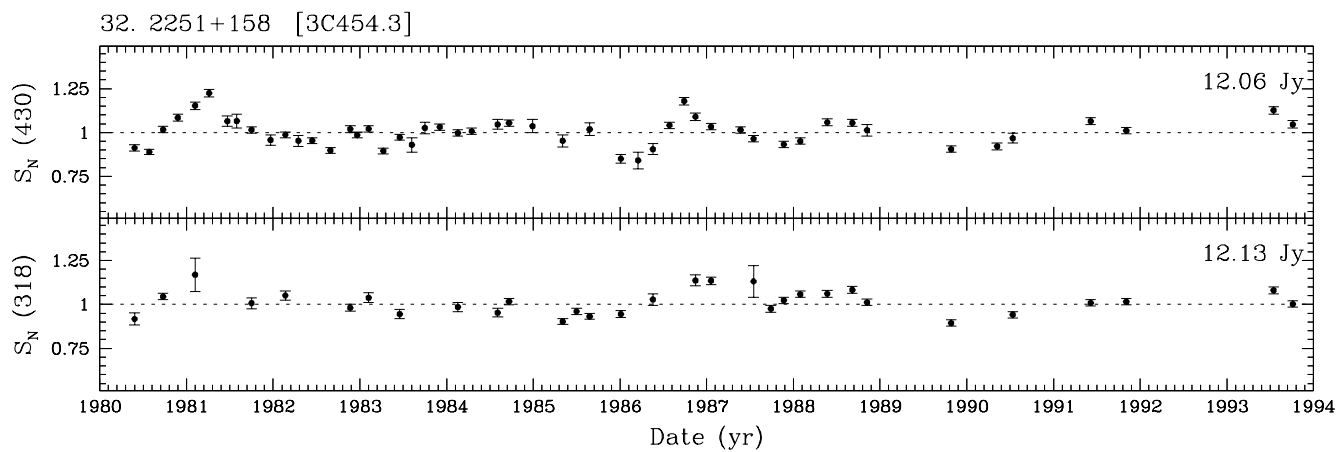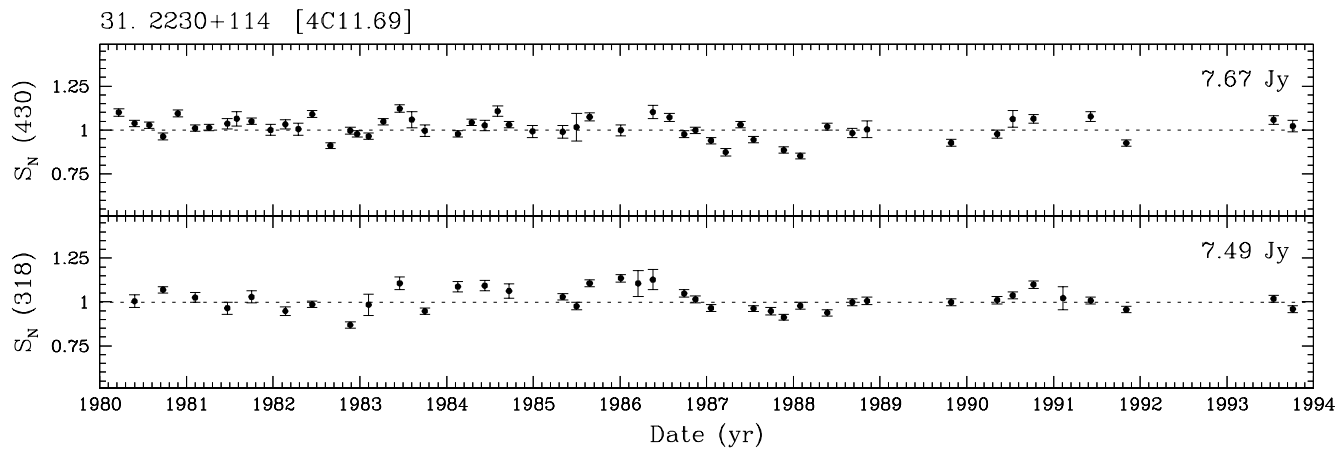
TABLE 2

Flux Densities, Modulation Indices, and Structure Function Classification

ID (1)	Source (2)	318 MHz							430 MHz						
		S^a (3)	MI (4)	Σ (5)	τ (6)	$V_L{}^b$ (7)	V_M (8)	V_Σ (9)	S^a (10)	MI (11)	Σ (12)	τ (13)	$V_L{}^b$ (14)	V_M (15)	V_Σ (16)
1	0038+328	9.81	0.030	NV					7.98	0.040	C				G
2	0056−001	4.56	0.058	NV		×	×		4.20	0.084	C		×	×	×
3	0116+319	4.09	0.042	NV					3.80	0.042	NV				
4	0202+149	5.46	0.056	B		×	×	×	5.49	0.052	B		×		×
5	0235+164	1.24	0.210	A	62	×	×	×	1.48	0.209	D	>80	×	×	×
6	0256+075	0.82	0.183	A	31	×	×	×	0.80	0.155	B		×		×
7	0316+162	6.74	0.045	A	46	×	×	×	6.96	0.089	D	>68	×	×	×
8	0333+321	3.11	0.115	A	67	×	×	×	3.08	0.118	C		×	×	×
9	0420−014	1.17	0.123	A	26	×		×	...	...	...	...			
10	0446+112	1.36	0.095	A	44	×		×	0.95	0.138	U^c		×		×
11	0723−008	3.25	0.112	B		×	×	×	2.52	0.101	A	24	×		×
12	0735+178	2.04	0.108	B		×	×	×	1.92	0.092	A	14	×		×
13	0736+017	1.93	0.170	B		×	×	×	2.38	0.142	A	30	×	×	×
14	0851+202	1.17	0.128	A	14	×	×	×	1.19	0.116	U^c		×		×
15	1039+029	7.46	0.030	NV					6.38	0.033	NV				
16	1055+018	5.12	0.071	A	16	×	×	×	4.46	0.053	A	6	×		×
17	1117+146	3.82	0.147	A	8	×	×	×	3.44	0.104	U^c		×	×	×
18	1345+125	8.11	0.044	NV		×	×		7.71	0.054	B		×	×	×
19	1422+202	5.57	0.040	NV					4.36	0.065	D		×	×	×
20	1548+056	2.57	0.099	A	18	×	×	×	2.52	0.066	U^c		×		×
21	1606+106	2.48	0.075	U^c		×	×	×	1.83	0.070	C		×		×
22	1611+343	3.37	0.170	C		×	×	×	2.90	0.204	C		×	×	×
23	1633+382	2.16	0.124	B		×	×	×	0.69	...	...	...	...		
24	1901+319	6.08	0.057	A	32	×	×	×	5.11	0.091	C		×	×	×
25	1922+333	7.32	0.032	NV					6.85	0.047	B		×		×
26	2050+364	2.91	0.049	A	28			×	3.09	0.196	A	16	×	×	×
27	2144+092	0.98	0.107	NV		×			1.04	0.111	C		×		×
28	2145+067	3.70	0.072	C		×	×	×	3.39	0.068	C		×		×
29	2201+315	3.30	0.051	C		×		×	2.91	0.070	C		×		×
30	2223+210	3.79	0.042	NV					3.24	0.057	C		×		×
31	2230+114	7.49	0.063	C		×	×	×	7.67	0.060	A	8	×	×	×
32	2251+158	12.13	0.071	C		×	×	×	12.06	0.079	A	8	×	×	×
33	2319+272	1.90	0.065	C		×		×	1.87	0.069	C		×		×
					Calibration Sources										
34	0127+233	8.55	0.011						6.60	0.024					
35	0528+064	13.08	0.014						9.86	0.020					
36	0710+118	11.37	0.019						8.55	0.021					
37	1005+077	18.87	0.006						15.44	0.013					
38	1328+254	15.29	0.010						13.14	0.028					
39	1328+307	27.18	0.010						24.49	0.025					
40	1756+134	6.88	0.010						5.79	0.018					
41	2203+292	9.62	0.015						7.28	0.042					

^{a} Weighted mean of flux densities (Jy). For calibration sources, the adopted flux densities (Jy).
^{b} Considered variable by one or more of the following determinations: visual inspection of the light curves (V_L), MI > 2MI$_c$ (V_M), and/or by structure-function analysis (V_Σ).
^{c} Undetermined.

TABLE 3

Adopted σ Values

ZA	σ_c	σ_g
	318 MHz	
<15°	0.0636	0.0199
>15°	0.0802	0.0191
	430 MHz	
<9°	0.0894	0.0218
>9°	0.1373	0.0198

However, we note that the modulation index criterion fails to identify sources 4, 6, 10, 11, 12, 14, 16, 20, 21, 25, 27, 28, 29, 30, and 33 as variable at 430 MHz, and sources 10, 27, 29, and 33 as variable at 318 MHz. An inspection of the light curves of all these sources reveals that they have larger measurement errors, but shows clear, often correlated, variability and classifiable structure-function types. At 318 MHz, source 2, 18, and 19 are found to be nonvariable by the structure-function criterion, whereas their modulation indices are greater than 2MI$_c$. This is due to single episodes of variation at epochs 1985.5, 1988.2, and 1984.7 in these sources. Such single episodes of deviant flux density are
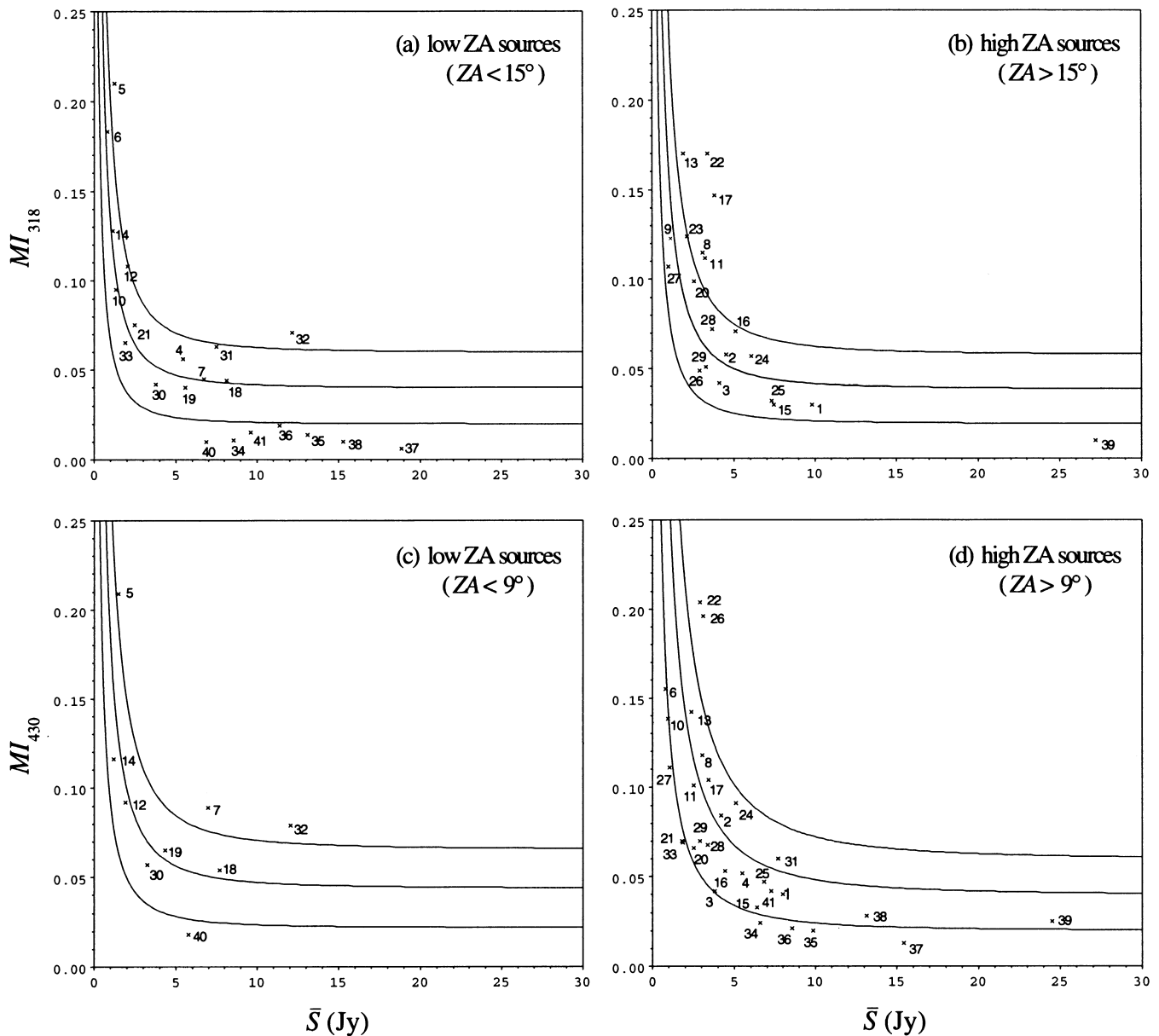
FIG. 3.—Derived modulation indices (MI) of all sources as a function of their weighted-mean flux densities. The lowest curve represents the error contribution computed using eq. (2). Additionally, $2MI_c$ and $3MI_c$ vs. flux density curves have been drawn.

more likely to cause a high modulation index value than a variable sourcelike appearance in the structure-function analysis.

According to all three criteria, we found that sources $0038 + 328$ (No. 1), $0116 + 319$ (No. 3), and $1039 + 029$ (No. 15) are nonvariable at both frequencies during the entire monitoring span. Source $2144 + 092$ (No. 27) is variable at 430 MHz according to the structure-function analysis. However, at 318 MHz, both the modulation index and the structure-function analysis fail to identify it as a variable, despite the source undergoing a variable phase before 1984. This phase is correlated with the one at 430 MHz during that time. Sources $1422 + 202$ (No. 19), $1922 + 333$ (No. 25), $2050 + 364$ (No. 26), and $2223 + 210$ (No. 30) are nonvariable at 318 MHz. Among these, $2050 + 364$ shows a highly striking behavior at 430 MHz, with indications of an extreme scattering event as observed for a few other sources at higher frequencies by Fiedler et al. (1987). This is discussed in more detail in the following section.

5. B2050 + 364

Among the sources that have shown significant variability over the monitoring period, B2050 + 364 displays unique behavior. Figure 2 (No. 26) shows our results for this source for over 10 yr of monitoring at 318 and 430 MHz. Between about 1985.75 and 1987.75, the 430 MHz flux density suddenly decreased from a relatively steady value of 3.3 Jy (a value also measured in 1981 October by Dennison et al. 1984) to a steady value of 2.25 Jy, returning to approximately 3.3 Jy after this period. We note that this behavior is not at all reflected in the 318 MHz monitoring data, where the flux density remained at a level of approximately 3 Jy over the whole period. Simultaneous 4.8, 8.0, and 14.5 GHz measurements made by H. D. Aller and M. F. Aller (1994, private communication) at Michigan do not show any significant variability at this time.

Although it is difficult to completely rule out an instrumental effect, we note that the time series for the sources
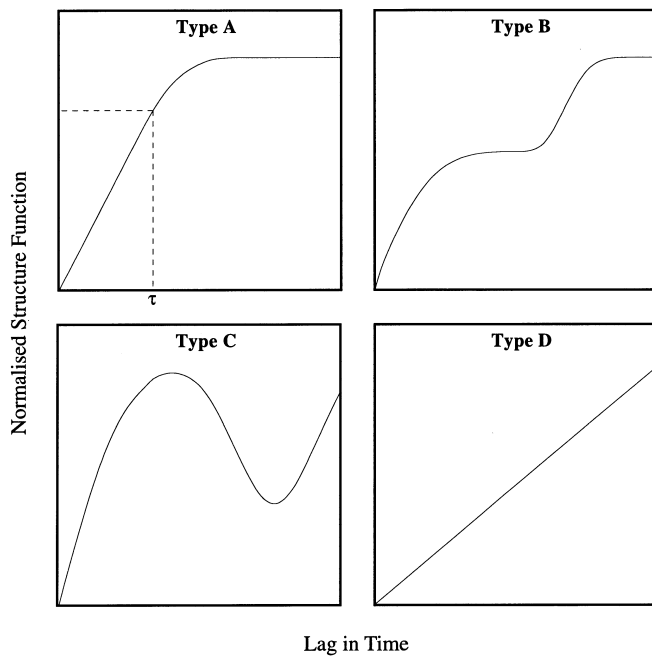
Fig. 4.—The structure-function classification scheme where type A represents a single variable component with time scale τ. Types B and C are probably cases where two or more independent components are contributing to the net intensity fluctuations; however, these could also be cases where more than a single physical process is involved (detailed modeling of these will constitute the material for a future paper). Type D represents very slowly varying sources.

observed immediately before and after $2050 + 364$, namely, $1922 + 33$ and $2144 + 09$, respectively, show no features that correspond to those measured for $2050 + 364$. In fact, no other source shows similar behavior. In addition,

$2050 + 364$ is the only source in our sample to be situated at such a low Galactic latitude ($l = 78°.9$, $b = -5°.1$), and an instrumental effect for it alone would constitute a remarkable coincidence. As the variability event was observed only at 430 MHz and neither at 318 MHz nor at higher frequencies, it is not believed that the variations could be intrinsic to the source. Furthermore, such a large variability event at such a low frequency suggests that it is a propagation effect. Preliminary interpretation of this result in terms of propagation effects has been presented by Altschuler et al. (1994). They suggest that, since the line of sight to $2050 + 364$ passes through the so-called Cygnus superbubble (Mutel & Lestrade 1988), it is quite possible for a plasma blob of sufficient electron density and appropriate size to move across the line of sight, causing an extreme scattering event similar to that observed by Fiedler et al. (1987) for a number of radio sources, including $0954 + 658$.

REFERENCES

Altschuler, D. R. 1989, Fundam. Cosmic Phys., 14, 37
Altschuler, D. R., Broderick, J. J., Condon, J. J., Dennison, B., Mitchell, K. J., O'Dell, S. L., & Payne, H. E. 1984, AJ, 89, 1784
Altschuler, D. R., Gurvits, L. I., Alef, W., Dennison, B., Graham, D., Trotter, A. S., & Carson, J. E. 1995, A&AS, 114, 197
Altschuler, D. R., Salgado, J. F., Dennison, B. K., & Ghosh, T. 1994, BAAS, 26, 1503.
Baars, J. W. M., Genzel, R., Pauliny-Toth, I. I. K., & Witzel, A. 1977, A&A, 61, 99
Biretta, J. A., Schneider, D. P., & Gunn, J. E. 1985, AJ, 90, 2508
Condon, J. J., Ledden, J. E., O'Dell, S. L., & Dennison, B. K. 1979, AJ, 84, 1
Dennison, B., Broderick, J. J., Ledden, J. E., O'Dell, S. L., & Condon, J. J. 1981, AJ, 86, 1604
Dennison, B., Thomas, M., Booth, R. S., Brown, R. L., Broderick, J. J., & Condon, J. J. 1984, A&A, 135, 19
Dent, W. A. 1965, Science, 148, 1458
Fiedler R. L., Dennison, B., Johnston, K. J., & Hewish, A. 1987, Nature, 326, 675

Hughes, P. A., Aller, H. D., & Aller, M. F. 1989, ApJ, 341, 54
Königl, A., & Choudhuri, R. 1985, ApJ, 289, 173
Marscher, A. P. 1992, in Physics of Active Galactic Nuclei, ed. W. Duschl & S. J. Wagner (New York: Springer), 510
Mitchell, K. J., Dennison, B., Condon, J. J., Altschuler, D. R., Payne, H. E., O'Dell, S. L., & Broderick, J. J. 1994, ApJS, 93, 441
Mutel, R. L., & Lestrade, J. F. 1988, AIP Conf. Proc. 174, Radio Wave Scattering in the ISM, ed. J. M. Cordes et al. (New York: AIP), 122
O'Dell, S. L., et al. 1988, ApJ, 326, 668
Rickett, B. J. 1986, ApJ, 307, 564
Sholomitskii, G. B. 1965, Soviet Astron., 9, 516
Spangler, S. R., Eastman, W. A., Gregorini, L., Mantovani, F., & Padrielli, L. 1993, A&A, 267, 213
Véron-Cetty, M. P., & Véron, P. 1993, A Catalogue of Quasars and Active Nuclei (6th ed.; ESO, Garching)
Wagner, S. J., et al. 1996, AJ, 111, 2187